Available online at www.sciencedirect.com
SCIENCE DIRECT®
Physics Letters A 339 (2005) 414–423
PHYSICS LETTERS A
www.elsevier.com/locate/pla

Observation of a low-field diamagnetic contribution to the magnetic susceptibility of deformed single crystal PdH_x ($x \simeq 4.0 \times 10^{-4}$)

Andrei G. Lipson [a,b], Brent J. Heuser [a,*], Carlos H. Castano [a], Ayten Celik-Aktas [a]

[a] *University of Illinois, Department of Nuclear, Plasma, and Radiological Engineering, Urbana, IL 61801, USA*
[b] *Institute of Physical Chemistry, Russian Academy of Sciences, 117915 Moscow, Russia*

Received 24 January 2005; accepted 17 March 2005

Available online 31 March 2005

Communicated by J. Flouquet

Abstract

Magnetic susceptibility measurements have been performed with deformed single-crystal Pd loaded with a low concentration of hydrogen. A diamagnetic contribution to the paramagnetic susceptibility of Pd has been observed below 30 K that is attributed to a condensed hydrogen phase at low temperature along dislocation cores in the deformed, single crystal Pd matrix.

PACS: 61.72.Lk; 61.72.Yx; 74.10.+v; 74.25.Ha

Keywords: Magnetic hysteresis; Hydrogen; Palladium; Dislocations

1. Introduction

Recently Ashcroft [1] has presented arguments that hydrogen–metal alloys, in particular dense hydrides of IVa group, may exhibit high temperature superconductivity (HTS) over a modest external pressure range. These arguments are based on similarities between electronic structure of hydrogen–metal alloys and the high temperature superconductor MgB_2 [2]. In Ashcroft's consideration, the feasibility of HTS in highly-loaded metal hydrides was related to metal–hydrogen band overlap increasing both the electron concentration and optical phonon energy. This resulted in strong electron–phonon coupling and the possibility of HTS. The advantage of IVa group hydrides for achieving HTS is that, in a chemical sense, these systems have undergone a form of pre-compression, and once impelled by further external pressure to enter metallic phase, the electrons from both hydrogen and metal may participate in common overlapping bands [1].

* Corresponding author.
E-mail address: bheuser@uiuc.edu (B.J. Heuser).

0375-9601/$ – see front matter
doi:10.1016/j.physleta.2005.03.052

There is another approach to achieve a compressed, metallic hydride state with a high coupling constant and this is the topic of the work presented here. Dislocation defects are strong, abundant traps of interstitial hydrogen and deuterium, as has been previously demonstrated in small angle neutron scattering (SANS) measurements [3]. In this past work it was found that dislocations in hydride-cycled, single crystal Pd were specific trapping sites for deuterium. Fits to the small-angle data yielded a trapping efficiency of 4–5 deuterons per Å of dislocation line length and a dislocation density of approximately 2×10^{11} cm^{-2} [3]. These measurements were performed at equilibrium at room temperature with a bulk concentration of 5.5×10^{-3} [D]/[Pd]. Non-equilibrium SANS measurements were also performed to investigate the effect of the deuterium-dislocation trapping interaction on the diffusive behavior [4]. Analysis of these data yielded a trapping energy of 0.2 eV. This result represents a concentration-weighted average over all trapping sites, including the weaker dislocation strain field sites far for the dislocation core [4,5]. Kirchheim investigated the dislocation trapping interaction at lower concentrations of residual hydrogen ($\sim 10^{-4}$ [H]/[Pd]) and found trapping energy of ~ 0.7 eV [6]. This energy suggests deep binding at dislocation core sites.

The local concentration of deuterium (hydrogen) at dislocations can be estimated from the equilibrium SANS results mentioned above. If the trapped deuterium is assumed to reside within approximately 10 Å of the dislocation core [3], and if the Pd atomic number density near the dislocation is assumed to be equal to the bulk density, the local deuterium concentration is approximately 0.2 [D]/[Pd]. This is considerably higher than the equilibrium bulk concentration specified above. The assumption regarding the Pd number density near dislocations is generally thought not to be correct, at least within one or two Burgers vectors of the core. Except for the broad statement that the host atomic density is significantly reduced at the cores of dislocation, the atomic density is not known [7]. In any event, the local deuterium (hydrogen) concentration near the dislocation core is likely much higher than 0.7 [D]/[Pd].

The pressure inside the cores of dislocations will be comparable with a palladium bulk modulus [7] (up to 180 GPa [8]) and the conditions of both hydrogen pre-compression and external pressure are essentially fulfilled. This is the basis for the above statement that a compressed metallic hydride state can be obtained via an alternative route—trapping at dislocation cores in deformed Pd. The electron properties of stoichiometric Pd hydride phases (with x greater than 1) have not been studied previously because these compounds are unstable at ambient conditions [9,10]. However, anomalies in the electron transport properties below 300 K in highly-loaded Pd hydrides have been reported [11–13]. The superconducting transition temperature of stable Pd hydrides is $T \sim 8$–9 K. It has been suggested that strong electron–phonon coupling to the optical modes, suppression of spin fluctuation in Pd lattice, and sd-hybridization of hydrogen and Pd electrons are involved in the superconducting transition [9,14].

In present the work, the magnetic properties of deformed, single crystal PdH_x with a very low overall loading ratio of $x = 4.0 \times 10^{-4}$ [H]/[Pd] were studied. Comparative magnetic measurements carried out with a 1 T SQUID indicate an appearance of a strong diamagnetic contribution to the paramagnetic response of the Pd matrix at temperatures below 30 K in a weak magnetic field ($H \leqslant 5.0$ Oe). In a higher magnetic field this phase exhibit an antiferromagnetic behavior with Curie–Weiss temperature $\theta = -29$ K.

2. Experimental

High purity (99.999%) Pd single crystal grown by Metal Crystals and Oxides of Cambridge, UK was employed in this work. The cylindrical ingot was grown by Czochralski method with a [110] cylinder axis, 10 cm in length and 1 cm in diameter. A sample with dimensions of $2.7 \times 2.7 \times 0.6$ mm^3 (corresponding mass of 52 mg) was cut from the as-grown ingot using a low speed diamond saw and mechanically polished to remove surface irregularities. This sample was annealed in a vacuum of 10^{-8} Torr at 800 °C for five hours. The magnetic susceptibility measurements of this annealed single crystal sample (without deformation or hydrogen loading) were performed and represent the background response of the Pd matrix.

Deformation of this same single crystal Pd sample was subsequently performed by cycling through the Pd–H miscibility gap. This cycling procedure is

known to create a relatively uniform dislocation substructure as incoherent phase boundaries pass through the sample [3,4]. Cycling was carried out by exposure to hydrogen gas at 930 Torr at 390 K for several hours in a closed volume of approximately 1 liter. The pressure reduction within the closed volume was monitored to determine when equilibrium was obtained, signaling the completion of the $\alpha \rightarrow \alpha'$ hydride phase transformation. The reverse phase transformation ($\alpha' \rightarrow \alpha$) was then induced by exposing the hydrogen-loaded sample to a vacuum of 10^{-6} Torr at 430 K for several hours.

The formation and decomposition of the hydride phase, as just described, represents one cycle across the miscibility gap in the Pd–H system. The sample used here was cycled twice. A final annealing step of the sample was performed at 573 K for two hours. This removed all but the most strongly trapped hydrogen, as discussed in the introduction and quantified below. Magnetic susceptibility measurements of the sample in this state represent the foreground response of the deformed Pd matrix with an overall hydrogen atomic ratio of 4.0×10^{-4} [H]/[Pd].

Magnetic measurements were carried out using a Quantum Design MPMS 1T-SQUID. The Pd sample, for both the background and foreground measurements, was placed in gelatin capsule and wrapped with a small piece of cotton. The orientation of sample was such that the long axes were normal to the direction of translation for the magnetic susceptibility measurements. Measurements with magnetic fluxgate showed that without an applied ultra-low field condition, the SQUID has residual magnetic field of $\Delta H \approx -0.2$ G. Ultra-low field installation with degaussing of the shielding produced a remnant field less than 1 mG. The sensitivity of SQUID was found to be higher than 5×10^{-8} emu based on a calibration measurement with the Pd standard at room temperature. The sample was cooled from 298 K to 2.0 K at $H = 0$ after zero field installation at room temperature to perform zero field cooling (ZFC) measurements of the magnetic moment. After the measurement of magnetic moment versus field, $M(H)$, at given temperature, the sample was heated at $H = 0$ to 350 K inside the SQUID. The cooling of Pd samples to the next chosen temperature was conducted at nominal $H = 0$ without zero field installation.

Thermal desorption analysis was used to estimate the residual hydrogen concentration in the sample after the magnetic susceptibility measurements were performed. The sample was heated from 20 °C to 930 °C at a constant rate 9.0 °C per minute in baseline vacuum of 10^{-8} Torr. The residual gasses released by the sample were recorded with a with Leybold Inficon Transpector quadrupole mass spectrometer. Calibration of the hydrogen release was done using a known mass of TiH_2 powder (approximately 0.1 mg) with a decomposition temperature near 400 °C.

3. Experimental results

A comparison of the thermal desorption analysis (TDA) measurements for the single crystal Pd sample with and without hydrogen is shown in Fig. 1. Both measurements were performed after the magnetic susceptibility measurements since the first TDA measurement removes all hydrogen. The without-hydrogen TDA measurement was performed immediately following the with-hydrogen measurement without removal of the sample from vacuum. The net area under the with-hydrogen curve after subtraction of the without-hydrogen curve was used to determine the overall hydrogen concentration in the sample, $x = 4 \pm 0.5 \times 10^{-4}$ [H]/[Pd]. The two curves shown in Fig. 1 terminate at 930 °C. This is the upper limit of the TDA system. Notice that the two curves are converging, a consequence of elevated H_2 background levels at high temperature and nearly complete outgassing of the foreground sample. The termination of the TDA measurements leads to an underestimation of the hydrogen concentration of roughly 10%, resulting in maximum possible concentration of 4.5×10^{-4} [H]/[Pd]. We do not consider this error to be significant given the uncertainty in the dislocation density and local Pd number density near dislocation, as discussed in the introduction.

The binding energy of hydrogen in the sample was estimated from the TDA data using the Garlic–Gibson model [15]. In this formalism, the activation energy for hydrogen release is given by

$$\varepsilon_{\mathrm{H}} = k_{\mathrm{B}} \frac{T_2 T_1}{T_2 - T_1} \ln(P_2/P_1), \tag{1}$$

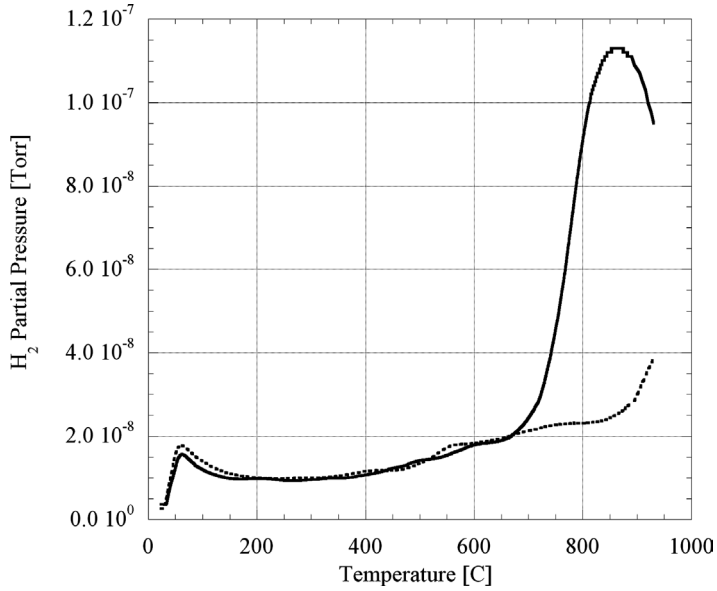

Fig. 1. Thermal desorption analysis measurements of single crystal Pd with (solid line) and without (dotted line) hydrogen. The same sample used for the magnetic moment measurements was used for the TDA measurements. The total hydrogen concentration and binding energy were determined from these data (see text).

where k_B is the Boltzmann constant and P_1/T_1 and P_2/T_2 are two points on the rising edge of the hydrogen release peak in the net TDA curve (not shown) so that $T_2 > T_1$ and $P_2 > P_1$. Here we equate the activation energy for release to the binding energy of the trapped hydrogen. The result of this analysis is $\varepsilon_H = 1.6 \pm 0.2$ eV. This binding energy is well above the enthalpy of Pd hydride formation ($|\Delta H| = 0.18$ eV [16]) and the activation energy for bulk diffusion ($E = 0.23$ eV [17]).

Thermal desorption analysis of the hydrogen trapping interaction at dislocations presented above indicates low residual hydrogen concentration and a large binding energy in the H-cycled single crystal Pd sample ($x = 4 \times 10^{-4}$ [H]/[Pd] and $\varepsilon_H = 1.6$ eV, respectively). These values represent the loaded state after a two hour anneal at 573 K. Unlike the case discussed in Refs. [3,4] (at an equilibrium concentration of 5.5×10^{-3} [D]/[Pd]) where the trapped deuterium was located at both core *and* elastic strain field sites, the residual hydrogen after annealing is at the strongest trapping sites. The high binding energy supports this conclusion. These sites will be within approximately one Burgers vector (2.75 Å) of the dislocation core, precisely where the host density is not known. The single crystal material and cycling procedure used here were the same as that used for the SANS work. However, the two-hour 573 K anneal was not performed in the previous work. We suspect this annealing procedure reduced the dislocation density by inducing a small amount of polygonization or overlap of the dislocation strain fields.

We can use the dislocation density from the SANS work to estimate a local hydrogen concentration at dislocations after the two hour 573 K annealing procedure. Accordingly to Maxelon et al. [5], the equation connecting the effective hydrogen concentration x_{eff} at the dislocation core to the segregation radius along the cylindrical dislocation core R_H is given by

$$x_{\text{eff}} = \frac{\alpha \langle [\text{H}]/[\text{Pd}] \rangle}{\pi \rho_d R_H^2}, \tag{2}$$

where $\alpha \sim 1.4$ is the factor counting the reduction in Pd atomic density along the dislocation. This factor can be estimated from core sites in deformed Pd as a/b, where a and b are the lattice constant and Burgers vector magnitude, respectively. Substitution of these parameters into Eq. (2) gives an upper limit of $x_{\text{eff}} = 1.35$, suggesting a superstoichiometric hydride formation at deep dislocation core sites in the H-cycled and 573 K annealed Pd single crystal.

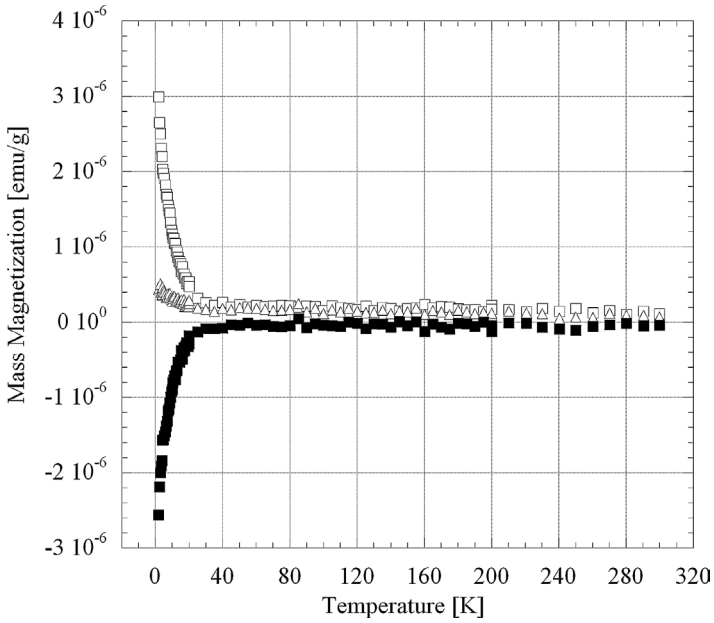

Fig. 2. DC mass magnetization versus temperature in a magnetic field of 0.5 Oe for annealed Pd (open boxes), PdH_x (open triangles), and net subtraction (solid boxes). The net data exhibit a diamagnetic contribution to the paramagnetic response of Pd.

The mass magnetization versus temperature in a weak field ($H = 0.5$ Oe) ZFC measurements of the foreground (PdH_x), background (annealed Pd), and net subtraction (PdH_x–Pd) are shown in Fig. 2. These data demonstrate that the magnetization of the hydrogen-loaded sample PdH_x is significantly lower than annealed single crystal Pd over the temperature range of $2 \leqslant T < 40$ K. The negative component of the magnetization represents, we believe, a diamagnetic contribution from a condensed hydrogen-rich phase along the dislocation cores in the deformed single crystal Pd matrix.

The dependence of the magnetic moment on external field was measured up to 200 Oe at several different temperatures in an effort to identify the origin of the diamagnetic contribution. The measurements of both samples at 2 K up to 10 Oe are shown in Fig. 3. The hysteretic behavior of both samples is evident, with the PdH_x sample exhibiting the strongest effect. This irreversible magnetization effect was observed at all temperatures below 298 K (not shown) and suggests the occurrence of a spin glass-like behavior possibly related to frustrated localized spin states.

The moment versus external field dependences in Fig. 3 have essentially different characters: (1) the total width ΔH of hysteresis loop at $M = 0$ of the PdH_x sample ($\Delta H = 7.5$ Oe) is much higher than that of the annealed Pd sample ($\Delta H = 3.7$ Oe); (2) the slope of the virgin part of hysteresis loop for PdH_x is lower than that for Pd; and (3) in contrast to the annealed Pd sample, the virgin part of magnetization curve of PdH_x has an inflection point at $H \sim 3.5$ Oe. This last observation could indicate non-paramagnetic behavior of the PdH_x sample. To verify this hypothesis the virgin curve of both samples was fit to the paramagnetic Langevin function [18]

$$M = M_0\big[\coth(\mu H/k_{\mathrm{B}}T) - (k_{\mathrm{B}}T/\mu H)\big],$$

where μ is the effective magnetic moment in units of Bohr magnetons, μ_{B}. These fits are shown in Fig. 4. The best fit to the initial magnetization curve for PdH_x yields $\mu = 0.24\mu_{\mathrm{B}}$, but does not successfully describe the $M(H)$ behavior. On the other hand, the initial magnetization curve for annealed Pd sample is satisfactorily fit with the Langevin function, resulting in $\mu = 0.27\mu_{\mathrm{B}}$. The value of this moment places an upper limit on Fe impurities at approximately 10 appm, consistent with the known purity of the original Pd ingot and is thought to be responsible for a low tem-

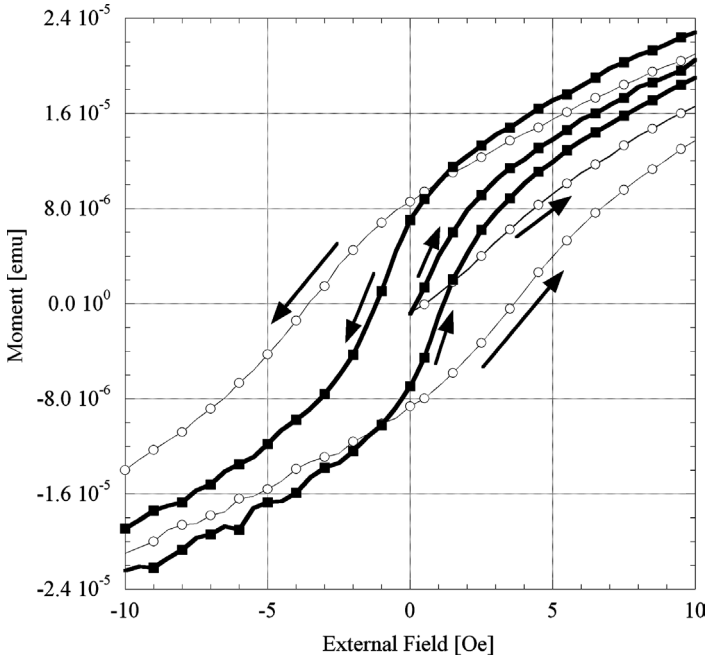

Fig. 3. Low-field magnetic moment versus external field for annealed Pd (solid boxes, thick lines) and PdH_x (open circles, thin lines) at 2 K. Both samples exhibit a hysteresis, with the PdH_x sample having the largest value.

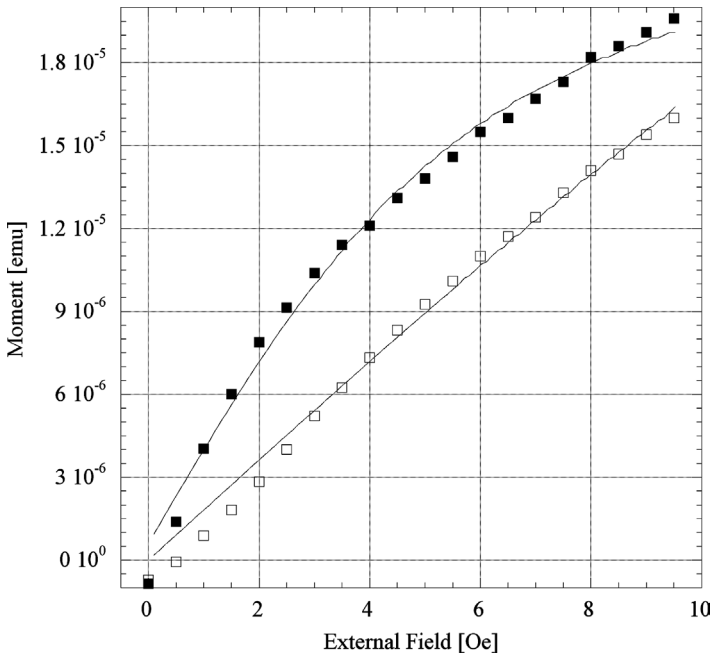

Fig. 4. Initial magnetic moment versus external field for annealed Pd (solid boxes) and PdH_x (open boxes). Fits to the Langevin equation describing the paramagnetic response are shown. The PdH_x sample is not well fit with this equation.

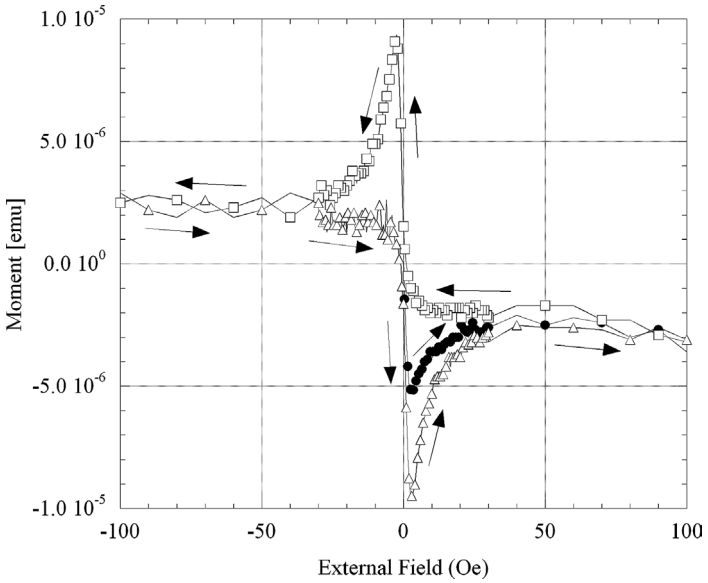

Fig. 5. Net magnetic moment (PdH_x–annealed Pd) versus external field for initial magnetization (solid circles), demagnetization (open boxes), and remagnetization (open triangles) at 2 K. Arrows indicate the direction of changing external field. The strong diamagnetic response at low field (< 5 Oe) and irreversible behavior are characteristic of a type II superconductor with flux pinning.

perature tails observed both in Pd (bgr) and PdH_x(fg) $M(T)$ curves in Fig. 2 [19].

The measured net moment (PdH_x–annealed Pd) as a function of external field obtained from the data shown in Fig. 3 is shown in Fig. 5. The net moment exhibits a minor hysteresis loop with a strong diamagnetic slope at low field (below approximately 5 Oe). This minor loop is superimposed on a broad diamagnetic "substrate" behavior with a much lower slope out to higher magnetic field. The detailed consideration of demagnetization part of the net $M(H)$ measurement showed a factor of four jump in the moment between 9.5 and 3.5 Oe when the magnetic field was reversed. The net magnetic moment behavior at 10 K (not shown) is similar to that at 2 K, but with a less noticeable inflection in the initial magnetization curve and a smaller diamagnetic slope at low field. At 50 K the differences in the hysteretic behavior between the Pd and PdH_x measurements (not shown) have all but disappeared, as has the inflection point in the PdH_x measurement. As a consequence, the minor loop hysteresis is absent.

The magnetic susceptibility as a function of temperature can be determined from the net $M(H)$ data recorded in this study (2.0, 10.0, 50.0, 100.0, and 298 K). This was done for both low ($H < 5$ Oe) and high ($10 < H < 100$ Oe) fields and is shown in Fig. 6. The low- and high-field susceptibilities are equivalent at 100 K and above. However, the low-field susceptibility exhibits a strong diamagnetic transition below approximately 50 K that is absent at high field. The net DC susceptibility of 15 nm Pd colloid particles derived from Ref. [20] is shown in Fig. 6 for comparison. Notice that the high-field net response from the PdH_x sample is similar to the Pd colloid response and differs only in absolute magnitude. The reduced paramagnetic susceptibility observed from colloidal Pd by Van Leeuwen et al. was attributed to a reduction in the Stoner factor that resulted from increased crystalline disorder in the nano-sized particles [20]. This explanation was based on earlier work by Meyer and Strizker which demonstrated that radiation-induced crystalline disorder causes a reduction in the susceptibility of Pd [21]. Van Leeuwen et al. developed a scaling law for the susceptibility versus Pd particle size [20]. Using this scaling law for our net data, we estimate a characteristic dispersion length of approximately $l \sim 60 \pm 15$ nm. In the present case this internal dispersity corresponds to the average dislocation spacing in cycled single crystal Pd given by $l \sim (9/\rho_d)^{1/2}$ [7] where

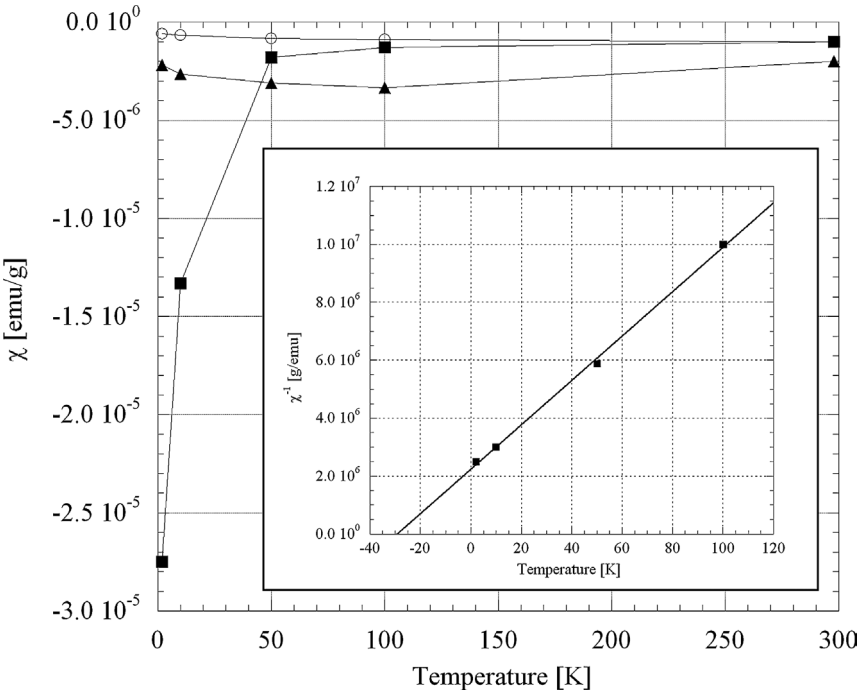

Fig. 6. Magnetic susceptibility versus temperature for the net data at high field (open circles), the net data at low field (solid boxes), and net 150 nm colloidal Pd (solid triangles) from Ref. [20]. The low-field net susceptibility exhibits a diamagnetic transition below 50 K. Inset shows inverse susceptibility versus temperature of net data at high field. The linear response is consistent with antiferromagnetic Curie–Weiss behavior.

ρ_d is the dislocation density. The dispersion length is therefore associated with a dislocation density of approximately 1.6–4.2 $\times 10^{11}$ cm^{-2}, in good agreement with the SANS measurements discussed in the introduction.

The high-field net susceptibility exhibits an antiferromagnetic Curie–Weiss behavior below 100 K. This is best seen in Fig. 6 inset, a plot of the inverse susceptibility versus temperature at high magnetic field assuming $\chi_0 = -1 \times 10^{-6}$ emu/g. These data are fit to the Curie–Weiss law, $\chi = \chi_0 + C/(T - \theta)$, where is the Curie–Weiss temperature [22], yielding $\theta = -29$ K. This value agrees well with the transition temperature $T_c \leqslant 30$ K observed in the net mass magnetization data in Fig. 2. The antiferromagnetic (AFM) behavior confirms that the irreversible $M(H)$ loops observed below 30 K (Figs. 3 and 5) cannot result, for example, from ordering of ferromagnetic impurities in Pd. The effect of such ordering on the magnetic susceptibility of a $PdFe_x$ ($x \sim 0.01$) alloy at low temperature has been observed in Ref. [21].

4. Discussion and summary of results

A few points of discussion exist related to the field and temperature dependencies of the magnetic measurements presented here.

1. The net magnetic moment at low temperature cannot be explained solely by the segregation of diamagnetic impurities in the PdH_x sample, including residual hydrogen. This is because the magnitude of this response is several orders greater than the diamagnetic contribution of residual hydrogen and other diamagnetic impurities [20]. In fact, Jamieson and Manchester did not observe a diamagnetic contribution to the Pd paramagnetic response for [H]/[Pd] below 0.01 [19].
2. The reduction in the paramagnetic response of the PdH_x sample compared to the annealed Pd sample cannot be explained by a dispersion effect, as has been observed in colloidal Pd particles. Although the net susceptibility at high field exhibits a behav-

ior similar to the colloidal Pd system, the low field data indicate a strong diamagnetic transition below 30 K that cannot be explained by a dispersion effect. This dispersion effect originates from a reduction in the Stoner factor, which is temperature and field independent. The diamagnetic transition observed here is clearly temperature and field dependent.

3. The low-temperature, low-field behavior of the initial magnetization of the PdH_x sample cannot be fit with the paramagnetic Langevin function, in contrast to annealed Pd sample. The total width of the hysteresis loop in the magnetic moment of the PdH_x sample is higher than annealed sample and increases non-linearly below 100 K (not shown). In addition, anomalies exist at low field in the demagnetization and remagnetization net response that correspond to the inflection point of the initial magnetization of the PdH_x sample. Thus, the resulting behavior of the net magnetization is not a result of a difference in paramagnetic responses.
4. The behavior of the initial magnetization of the PdH_x sample cannot be attributed to redistribution of ferromagnetic impurities in the Pd sample induced by hydride cycling. This is because the net susceptibility at high field exhibits an antiferromagnetic behavior below 100 K. However, the effect of PdH_x irreversible magnetization observed below 100 K cannot, in principle, rule out the occurrence of a spin-glass behavior (in coexistence with antiferromagnetism [23]), reflecting the frustrated nature of Pd/PdH_x nanoparticles as localized spins [18].

We therefore consider the strong diamagnetic contribution observed at low temperature and low magnetic field to be anomalous, inconsistent with explanations related to ferromagnetic impurities and residual interstitial hydrogen. In the absence of these explanations, we attribute the net diamagnetic response to the condensation of a hydrogen-rich phase at or near dislocation cores in the deformed Pd matrix. The behavior of the net magnetic moment in Fig. 5 is characteristic of a type II superconductor with a lower critical field of $H_{C1} \sim 3.5$ Oe. However, this behavior is not ideal since it is not reversible, but instead it exhibits the irreversible effects of flux pinning. Flux pinning in this case is a natural consequence of the condensation of the hydrogen-rich superconducting phase at dislocation defects. Notice that AFM ordering and superconducting properties may often coexist in type II superconductors, such as Pd-nanoparticles/graphene sheets [22] and high temperature superconducting curates [24]. In those cases, the AFM state can exist only at higher field because at lower field the fluctuations destroy the long range AFM order [24].

The critical temperature T_C for the hydrogen-rich superconducting phase can be estimated from the following relation [1]:

$$T_C = \frac{\langle \hbar\omega \rangle}{1.2k_B} \exp\left[\frac{-1.04(1+\lambda)}{\lambda - \mu^*(1+0.62\lambda)}\right], \tag{3}$$

where $\langle \hbar\omega \rangle$ is the characteristic average of phonon energy in the condensed phase, $\lambda_{ep} = \lambda(\mathrm{Pd}) + \lambda(\mathrm{H})$ is the electron–phonon coupling constant and represents the sum from the Pd and hydrogen subsystems, and μ^* is the Coulomb pseudopotential that accounts for the repulsive effect between electrons.

The magnitude of the electron–phonon coupling constant $\lambda(\mathrm{H})$ was found to be exactly proportional to the $x = [\mathrm{H}]/[\mathrm{Pd}]$, at least in the range of $0.8 < x < 1.0$, while the Pd contribution $\lambda(\mathrm{Pd})$ did not depend on concentration [14,25]. Assuming a linear dependence of $\lambda(\mathrm{H})$ on the [H]/[Pd] ratio above $x = 1.0$ and using values $\lambda_{ep} = 0.56$ and $\lambda(\mathrm{Pd}) = 0.143$ calculated for PdH_1 [13], we obtain $\lambda_{ep} = 0.643$ for $x_{eff} = 1.35$. Substituting an average characteristic phonon energy of $\langle \hbar\omega \rangle \sim 58$–$105$ meV (corresponding to the phonon energy range of a highly loaded Pd-black [26,27]) and $\mu^* \sim 0.1$–0.13 [1,14,25] into Eq. (3), we find the value of T_C for the $PdH_{1.35}$ compound at dislocation cores is in the range of $18 \leqslant T_C < 42$ K. This range is in good agreement with the diamagnetic transition observed here below 30 K.

The anomalous diamagnetic response observed in this work is an indication, we believe, of weak superconductivity in deformed Pd matrix. This superconductivity is attributed to a condensed hydrogen-rich quasi-metallic phase at dislocation defects where both hydrogen and palladium atoms participate in common overlapping bands [1]. The diamagnetic response has not observed directly, but rather only after subtraction. This is a consequence of the very low volume fraction of the deformed Pd sample participating in the superconducting phase transition (of order 10^{-4}). In other words, the absence of direct evidence for the diamag-

netic effect characterizing type II superconductor is the result of a very small contribution of diamagnetic response from the hydrogen-rich phase inside deep dislocation cores compared to the entire PdH_x paramagnetism response. Similar magnetic behavior from a minute superconducting fraction of $\sim 5 \times 10^{-4}$ at $T = 1.9$ K ($T_C \sim 3.6$ K) for Pd nanoparticles sandwiched between graphene sheets (Pd–MG) was recently demonstrated by Suzuki et al. [22]. An effect that could mask a direct diamagnetic response in PdH_x is the paramagnetic Meissner effect. This effect would be due to the sub-micrometer size mosaic structure of our samples after the hydrogen cycling. These inhomogeneities can result in magnetic flux capture at the mosaic boundaries, resulting in a paramagnetic response below T_C at low field FC [28,29] and even in ZFC [30] measurements [30].

Work is underway to increase the volume fraction of condensed hydrogen phase thought to exist along dislocation cores in PdH_x.

Acknowledgements

This work was partially support by the NSF under Grant No. DMR-9982520. The magnetic susceptibility measurements were performed at the Center for Microanalysis of Materials at the Frederick Seitz Material Research Laboratory at UIUC. This facility is supported by the US Department of Energy under Grant No. DEFG02-91-ER45439. The authors would like to thank Mr. T. Banks (UIUC) for his help with the magnetic susceptibility measurements, Dr. A. Bezryadin (UIUC) for overall interest in this work, and Dr. R. Prozorov (Univ. South Carolina) for his valuable comments on magnetic measurement results.

References

[1] N.W. Ashcroft, Phys. Rev. Lett. 92 (2004) 187002.
[2] J. Nagamatsu, et al., Nature (London) 410 (2001) 63.
[3] B.J. Heuser, J.S. King, J. Alloys Compd. 261 (1997) 225.
[4] B.J. Heuser, J.S. King, Metal. Mat. Mater. Trans. A 29 (1998) 1594.
[5] M. Maxelon, et al., Acta Mater. 49/14 (2001) 2625.
[6] R. Kirchheim, Acta Metall. 29 (1981) 845.
[7] J.P. Hirth, J. Lothe (Eds.), Theory of Dislocations, second ed., Krieger, Malabar, FL, 1982.
[8] G. Elsasser, K.M. Ho, C.T. Chan, M. Fahnle, J. Phys.: Condens. Matter 4 (1992) 5207.
[9] B. Strizker, H. Wuhl, in: G. Alefeld, J. Völkl (Eds.), Hydrogen in Metals II, in: Topics in Applied Physics, vol. 29, Springer-Verlag, Berlin, 1978.
[10] L. Schlapbach, I. Anderson, J.P. Burger, in: K.H.J. Buschow (Ed.), Material Science and Technology, vol. 3B, Part II, Weinheim, New York, 1994, p. 287.
[11] C. Herrero, F.D. Manchester, Phys. Lett. A 86 (1981) 29.
[12] P. Tripodi, F. Tanzella, M.H.C. McKubre, et al., Phys. Lett. A 276 (2000) 1.
[13] A.G. Lipson, B.F. Lyakhov, D.M. Sakov, V.A. Kuznetsov, Phys. Solid State 39 (1997) 1891.
[14] J.M. Rowe, J.J. Rush, J.E. Schriber, J.M. Nintz, Phys. Rev. Lett. 57 (1986) 2955.
[15] G.F.J. Garlick, A.F. Gibson, Proc. R. Soc. London, Sect. A 60 (1948) 574.
[16] R. Lässer, K.-H. Klatt, Phys. Rev. B 28 (1983) 748.
[17] J. Völkl, G. Alefeld, in: G. Alefeld, J. Völkl (Eds.), Hydrogen in Metals I, in: Topics in Applied Physics, vol. 28, Springer-Verlag, Berlin, 1978.
[18] D. Mendoza, F. Morales, R. Escudero, J. Walter, J. Phys.: Condens. Matter 11 (1999) L317.
[19] H.C. Jamieson, F.D. Manchester, J. Phys. F: Metal. Phys. 2 (1972) 323.
[20] D.A. Van Leeuwen, J.M. Van Reitebeek, G. Schmidt, L.J. De Jongh, Phys. Lett. A 170 (1992) 325.
[21] B. Meyer, B. Strizker, Phys. Rev. Lett. 48 (1982) 502.
[22] M. Suzuki, I.S. Suzuki, J. Walter, J. Phys.: Condens. Matter 16 (2004) 903.
[23] S. Majumdar, E.V. Sampathkurmaran, Phys. Rev. B 62 (2000) 8959.
[24] D. Knopp, et al., Phys. Rev. B 71 (2005) 064504.
[25] D.A. Papaconstantopoulos, B.M. Klein, E.N. Economou, L.L. Boyer, Phys. Rev. B 17 (1978) 141.
[26] J.M. Nicol, J.J. Rush, R.D. Kelley, Phys. Rev. B 36 (1987) 9315.
[27] N. Nishimiya, T. Kishi, T. Mizushima, et al., J. Alloys Compd. 319 (2001) 312.
[28] A.K. Geim, et al., Nature 396 (1998) 144.
[29] S. Reidling, et al., Phys. Rev. B 49 (1994) 13283.
[30] S. Yuan, L. Ren, F. Li, Phys. Rev. B 69 (2004) 092509.